PHYSICAL REVIEW B **95**, 041112(R) (2017)

Self-energies in itinerant magnets: A focus on Fe and Ni

Lorenzo Sponza, Paolo Pisanti, Alena Vishina, Dimitar Pashov, Cedric Weber, and Mark van Schilfgaarde
King's College London, London WC2R 2LS, United Kingdom

Swagata Acharya
Indian Institute of Technology, Kharagpur 721302, India
and King's College London, London WC2R 2LS, United Kingdom

Julien Vidal
EDF R&D, Department EFESE, 6 Quai Watier, 78401 Chatou, France

Gabriel Kotliar
The State University of New Jersey, 136 Frelinghuysen Road, Piscataway, New Jersey 08854, USA
(Received 21 March 2016; revised manuscript received 6 December 2016; published 26 January 2017)

We present a detailed study of local and nonlocal correlations in the electronic structure of elemental transition metals carried out by means of the quasiparticle self-consistent GW (QS*GW*) and dynamical mean field theory (DMFT). Recent high resolution ARPES and Haas-van Alphen data of two typical transition metal systems (Fe and Ni) are used as a case study. (i) We find that the properties of Fe are very well described by QS*GW*. Agreement with cyclotron and very clean ARPES measurements is excellent, provided that final-state scattering is taken into account. This establishes the exceptional reliability of QS*GW* also in metallic systems. (ii) Nonetheless QS*GW* alone is not able to provide an adequate description of the Ni ARPES data due to strong local spin fluctuations. We surmount this deficiency by combining nonlocal charge fluctuations in QS*GW* with local spin fluctuations in DMFT. (iii) Finally we show that the dynamics of the local fluctuations are actually not crucial. The addition of an external static field can lead to similarly good results if nonlocal correlations are included through QS*GW*.

DOI: 10.1103/PhysRevB.95.041112

High-resolution spectroscopy is limited in transition metals, in part because it is difficult to make sufficiently high quality samples. Fe and Ni are elements of which high quality films have been grown, and high-resolution angle-resolved photoemission spectroscopy (ARPES) performed [1]. These experiments provides a good reference to test the validity of different approximations of the electronic structure.

There are also not many calculations of spectral functions in these materials. Fe has been studied in the local-density approximation (LDA) [2] and with corrections through dynamical-mean field theory (DMFT) [3]. It is not surprising that the LDA does not track the ARPES experiment well [4], but it has been found that LDA+DMFT also fails to properly account for ARPES data [3]. The *GW* approximation [5] is widely applied to many kinds of insulators, but how well it describes 3*d* transition metals is much less established.

Through quasiparticle self-consistency (QS*GW*) one determines the noninteracting Green's function G_0 which is minimally distant from the true Green's function G [6–8]. Within QS*GW* many electronic properties are in excellent agreement with experiment [6], most notably the quasiparticle band structures. Moreover, at self-consistency the poles of QS*GW* $G_0(\mathbf{k},\omega)$ coincide with the peaks in $G(\mathbf{k},\omega)$. This means that there is no many-body "mass renormalization" of the noninteracting Hamiltonian, which allows for a direct association of QS*GW* energy bands $E(\mathbf{k})$ with peaks in the spectral function $A(\mathbf{k},\omega)$. Thus, QS*GW* provides an optimum framework to test the range of validity and the limitations to the *GW* approximation.

In this Rapid Communication, we compare QS*GW* results to various experimental data in elemental 3*d* materials in the Fermi liquid (FL) regime, with a heavy focus on Fe because of the high quality of ARPES [1] and de Haas-van Alphen (dHvA) [9,10] data available. We will show that QS*GW* and ARPES spectral functions agree to within experimental resolution, with the proviso that the final state scattering is properly accounted for in interpreting the experimental data. By contrast, discrepancies appear in Ni—a classical itinerant ferromagnet. This can be attributed to the lack of spin fluctuations in *GW* diagrams. However we find out that there is no need to include finite-energy spin fluctuations, instead a static correction to the QSGW self-energy is sufficient to correct for the size of the local moment. This findingopens up an avenue to test the validity of a similar argument for other transition metals. The LDA or LDA+DMFT should be problematic, as nonlocality in the self-energy can be important (see Supplemental Material).

I. FE IN THE FERMI LIQUID REGIME

Figure 1 compares the calculated QS*GW* band structure of Fe to peaks in ARPES spectra of Ref. [1], along with some inverse photoemission data [11]. While agreement appears to be very good, there are some discrepancies, particularly along the Γ-H line [see also Fig. 2(a)]. As noted earlier, the QS*GW* band structure reflects the peaks of $A(\mathbf{k},\omega)$ with no renormalizations from the ω or $\mathbf{k}$ dependence of Σ.

In the FL regime, ARPES spectra $I(\mathbf{k},\omega)$ are generally thought to be a fairly direct measure of $A(\mathbf{k},\omega)$. But the two

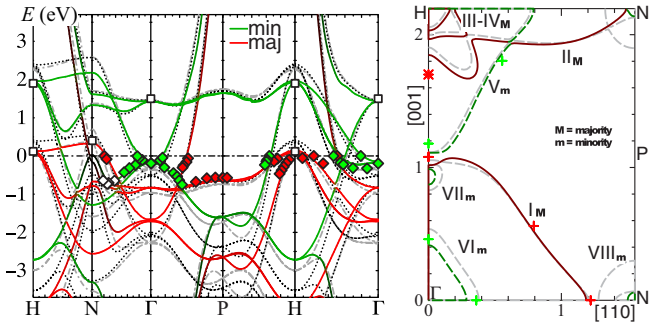

FIG. 1. Left: QS*GW* band structure of Fe (solid lines), LSDA (gray dashed), k-point averaged QS*GW* (black dotted, see text), ARPES spectra [1] (diamonds), and inverse photoemission spectra [11] (squares). Right: Fermi surface. Symbols denote FS crossings reported in Ref. [1]. Red and green depict majority and minority d character, respectively.

are not identical even in the FL regime, independently of the precision of the experimental setup. Assuming a one-step model [12] for the photoemission process (initial and final state coupled through Fermi's golden rule [12,13]) $I(\mathbf{k},\omega)$ can be written as

$$I(\mathbf{k},\omega) \propto \int d k_\perp |T_{fs}|^2 |M_{fi}(\mathbf{k}_\perp)|^2 A_f(\mathbf{k}_\perp) A(\mathbf{k},\omega),$$

$$\text{where } A_f(\mathbf{k}_\perp) = \frac{\Delta k_\perp / 2\pi}{(\Delta k_\perp/2)^2 + (k_\perp - k_\perp^0)^2} \qquad (1)$$

is the spectral function of the final state, broadened by scattering of the photoelectron as it approaches the surface [14]. T_{fs} is the final-state surface transmission amplitude and M_{fi} the photoexcitation matrix element (taken to be constant and

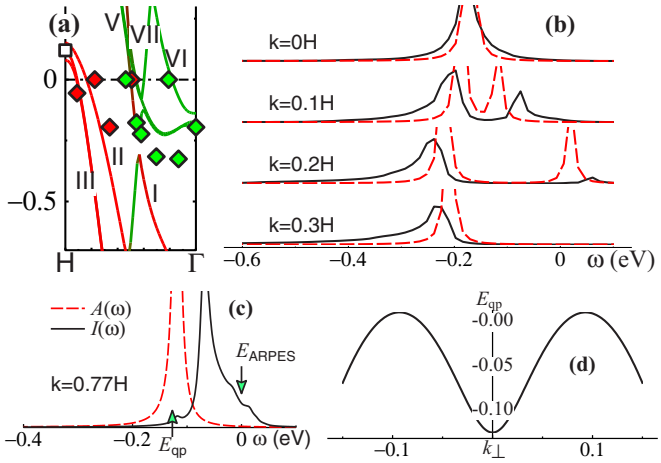

FIG. 2. (a) The Γ-H line of Fig. 1 in high resolution. Labels correspond to traditional assignments of Fermi surface pockets [1,9]. (b) Dashed line is QS*GW* spectral function $A(k,\omega)$ for various points on the Γ-H line, with $\mathsf{k}=0$ and $\mathsf{k}=1$ denoting Γ and H. Solid line is $A(\omega)$ modified according to Eq. (1). (c) The analog of (*b*) at $k = 0.77 \times \mathsf{H}$ where the II_M band crosses E_F. E_QP indicates the QS*GW* QP level, and E_ARPES the experimental ARPES peak at 0.77H. (d). dispersion in the QS*GW* II_M band on a line $\mathbf{k}_\perp + [0,0,0.77\mathsf{H}]$ normal to the film surface.

k independent [15]). Thus the final state is considered to be a damped Bloch wave, taking the form of a Lorentzian distribution centered in $k_\perp^0$ and broadened by $\Delta\mathbf{k}_\perp$ [14], while the initial state is an undamped Bloch function with an energy broadening ΔE, obtained through the QS*GW* spectral function. This approximation is reasonable since in the FL regime $A(\mathbf{k},\omega)$ is sharply peaked around the QP level. $\Delta\mathbf{k}_\perp$ is directly related to the inverse of the electron mean free path. For photon energy in the range 100–130 eV, $\Delta\mathbf{k}_\perp \approx 0.2$ Å^{-1} [16,17].

The final-state scattering broadens $I(\omega)$, but it also can shift the peak $\bar{\omega}$ in $I(\omega)$. The most significant discrepancy between ARPES and QS*GW* is found in the V_m band, Fig. 2(a) between $k=0$ and $0.4 \times \mathsf{H}$. Figure 2(b) shows $A(\mathbf{k},\omega)$ calculated by QS*GW*, and the corresponding $I(\mathbf{k},\omega)$ calculated from Eq. (1). Estimating the peak shift change from $\delta\bar{\omega} = \int d\omega\, \omega I / \int d\omega I - \int d\omega\, \omega A / \int d\omega A$, we find $\delta\bar{\omega} < 0.01$ eV at Γ, increasing to $\delta\bar{\omega} \approx 0.06$ eV for k between 0.1H and 0.3H. $\delta\bar{\omega} = 0.06$ eV tallies closely with the discrepancy between the V_m band and the measured ARPES peak for $0.1\mathsf{H} < k < 0.3\mathsf{H}$. There is also a significant discrepancy in the II_M band near $k = 0.77 \times \mathsf{H}$. Where it crosses E_F, the QS*GW* bands deviate from the ARPES peak by nearly 0.15 eV. But ARPES simulated by Eq. (1) is much closer to experiment [Fig. 2(c)]. This is understood from Fig. 2(d), which plots the QS*GW* dispersion along a line $\Delta\mathbf{k}_\perp$ normal to the film surface, passing through [0,0,0.77H]. A measurement that includes contributions from this line biases the ARPES peak in the direction of E_F since $\mathrm{E_{qp}}$ is minimum at $k_\perp$=0. Thus we attribute most of the discrepancy in the Fermi surface crossing [red star in Fig. 1(b)] to an artifact of final-state scattering.

To better pin down the errors in QS*GW*, we turn to de Haas-van Alphen (dHvA) measurements. Extremal areas of the FS cross sections can be extracted to high precision from dHvA and magnetoresistance experiments. Areas normal to [110] and [111] are given in Table I, along with areas calculated by QS*GW*. Figure 1 shows the QS*GW* Fermi surface, which closely resembles the one inferred by Lonzarich (version B) [19]. There is some ambiguity in resolving the small $\mathrm{VIII_m}$ pocket at N because its tiny area is sensitive to computational details. Discrepancies in the extremal areas are not very meaningful: It is more sensible to determine the change ΔE_F in Fermi level needed to make the QS*GW* area agree with dHvA measurements. This amounts to the average error in the QS*GW* QP levels, assuming that the bands shift rigidly. This assumption is well verified for all pockets, except for the small VI one owing to strong electron-phonon coupling [20].

Some limited cyclotron data for effective masses are also available [18], which are expected to be more reliable than ARPES data. It is seen that agreement is excellent (Table I, bottom panel) except for the small VI pocket. We get a better comparison by accounting for the electron-phonon coupling with a simple model [20,21]. From the model, v_F is renormalized by a factor $1+\lambda = 1.6$, which reasonably accounts for discrepancy between the QS*GW* and the cyclotron mass in pocket VI. The other pockets are much larger [Fig. 1(b)], making v_F much larger on average and the renormalization smaller.

Such a perfect agreement with experiments could not be possible without the accurate description of nonlocal components in the QS*GW* self-energy. To prove this statement

TABLE I. de Haas-van Alphen measurements of extremal areas A on the [110] and [111] Fermi surfaces, in Å^{-2}. ΔE_F is an estimate of the error in the QP level (eV), as described in the text. Bottom panel: cyclotron mass, $m^*/m = (\hbar^2/2\pi m)\,\partial A/\partial E$.

FS	dHvA [110]			dHvA [111]		
pocket	QS*GW*	expt. [9]	ΔE_F	QS*GW*	expt. [9]	ΔE_F
I	3.355	3.3336	0.01	3.63	3.5342	0.04
II				3.694		
III	0.2138	0.3190	0.05	0.1627	0.2579	0.06
IV	0.0897	0.1175	0.04	0.0846	0.1089	0.02
VI	0.3176	0.5559	−0.13	0.2799	0.4986	−0.14
VII	0.0148	0.0405	0.04			
		m/m* [110]			*m*/m* [111]	
	QS*GW*	LDA	expt. [18]	QS*GW*	LDA	expt. [18]
I	2.5	2.0	2.6			
V				−1.7	−1.2	−1.7
VI				2.0	1.5	2.8

we computed the band structure with a local potential obtained from a k-point average of the QS*GW* self-energy. The result is reported as a dotted black curve in Fig. 1, to be compared with the pale gray lines of LSDA and the solid lines of QS*GW*. The k-averaged potential reproduces a band structure that is much closer to the LSDA one than to the QSGW results. This results in the overestimation of the binding energy, e.g., of most states close to Fermi (for instance at Γ), or in the range between −2 and −3 eV (see at Γ, P, and H). An additional verification that local physics is not relevant in the description of the quasiparticle structure of Fe can be found in the Supplemental Material [20].

II. NI: AN ARCHETYPICAL ITINERANT MAGNET

Less detailed information is available for other elemental transition metals. We have extracted some experimental bandwidths and also the exchange splitting ΔE_x in the magnetic elements. Figure 3(a) shows that both seem to be very well described by QS*GW*, except that ΔE_x deviates strongly from experiment in Ni. QS*GW* significantly improves not only on the LSDA, but also on fully self-consistent *GW* [22] because of loss of spectral weight in fully self-consistent G that is avoided in QS*GW* [6].

Figure 4(a) compares the QS*GW* band structure of Ni to ARPES data [23]. Agreement is excellent in the minority channel, but ΔE_x is uniformly too large on the symmetry lines shown. Also the band near −1 eV at L (consisting of s character there) is traditionally assumed to be a continuation of the d band denoted as white and green diamonds, but the calculations show that at it is a continuation of the Ni s band. The corresponding LSDA band (light dotted lines) crosses L at E_F−0.44 eV; also the d bands are much wider.

ΔE_x is about twice too large in both QS*GW* and the LSDA, and for that reason spin wave frequencies are also too large [24]. Spin fluctuations $\langle M^2\rangle$ are important generally in itinerant magnets but they are absent in both LSDA and QS*GW*. One important property they have is to reduce the average magnetic moment $\langle M\rangle$ and hence to quench ΔE_x [25,26]. Figure 3(b) shows this trend quite clearly: Systems such as Fe, Co, and NiO are very well described by QS*GW*, but M is always overestimated in itinerant magnets such as FeAl, Ni_3Al, and Fe based superconductors such as $BaFe_2As_2$. Ni is

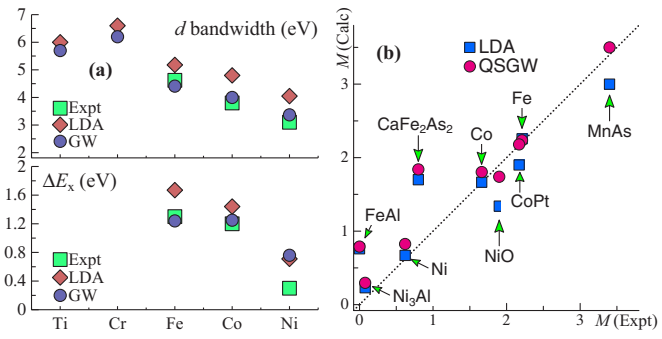

FIG. 3. (a): d bandwidth (top panel) and exchange splitting ΔE_x (bottom panel) in the 3d elemental metals. (b): Magnetic moment of several compounds

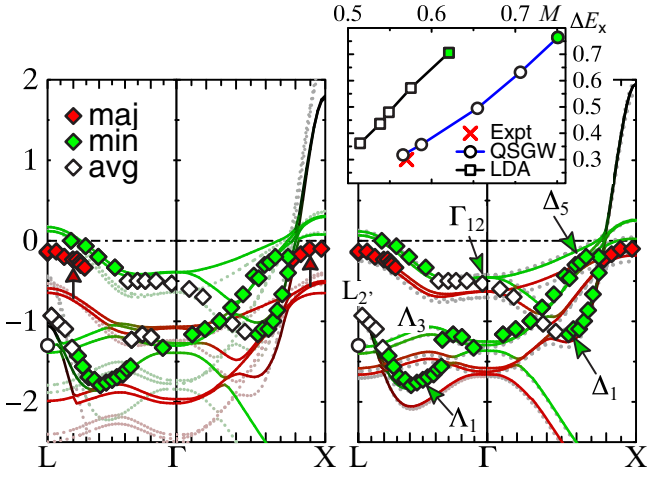

FIG. 4. (left) Band structure of Ni in QS*GW* (solid lines) and LDA (dotted) and ARPES data [23] (the circle at −1.3 eV was taken from Ref. [27]). Red arrows highlight the discrepancy in the exchange splitting ΔE_x at near L and X. (right) QS*GW*+LSDMFT bands (solid) and QS*GW*+$B^{\rm eff}$ (dashed). (inset) ΔE_x at L as a function of M obtained by adding an external magnetic field to the QS*GW* or LSDA potential (see text).

TABLE II. Magnetic moment M and exchange splitting ΔE_x for the different levels of the theory (see text) against experiment.

	M (Bhor)	ΔE_x @ L (eV)
LSDA	0.62	0.71
QSGW	0.75	0.77
QSGW+DMFT	0.51	0.30[a]
QSGW+SLDMFT	0.53	0.30
QSGW+B^{eff}	0.57	0.32
Experiment	0.57	0.31

[a]Value estimated from Maximum entropy analytic continuation.

also itinerant to some degree (unlike Fe, its average moment probably disappears as $T \to T_c$), and its moment should be overestimated. This is found to be the case for QSGW, as Fig. 3(b) shows.

Local spin fluctuations are well captured by localized nonperturbative approaches such as DMFT. We can reasonably expect that the addition of spin-flip diagrams to QSGW would be sufficient to incorporate these effects. A G_0W_0+DMFT study of ferromagnetic Ni can be found in Ref. [28], but the dependency of G_0W_0 on the starting point, together with all the advantages mentioned at the beginning, motivated us to devise a QSGW-based approach.

Here we adopt an implementation merging QSGW with DMFT. We adapted Haule's continuous time quantum Monte Carlo solver [29,30] with the projection and embedding schemes described in Ref. [31], and which are outlined in the Supplemental Material [20]. In this sense, this method is close to the one introduced by some of us in [32], but based on a different self-consistent scheme for the solution of the weakly correlated part.

The fully consistent QSGW+DMFT calculation is composed by alternately repeated DMFT and QSGW loops. First the QSGW Green's function is converged at fixed density, then it is projected on the Ni d orbitals and finally, within the DMFT loop, the local self-energy is obtained. Updating the total density with the locally corrected Green's function and repeating the procedure leads to complete self-consistency. This method fully takes into account the dynamics of the local spin fluctuations included in the DMFT diagrams. Results are reported in Table II and they confirm that DMFT adds the correct local diagrams missing in the QSGW theory. Moreover by carefully continuing the resulting Green's function on the real-frequency axis, we find an exchange splitting of $\sim$0.3 eV and a satellite at $\sim$5 eV [20].

In order to investigate the importance of the dynamics in the local spin-spin channels, we carry out a QSGW+DMFT calculation by retaining only the static limit of the DMFT loop (we call it QSGW+"SLDMFT"). Once the DMFT loop converges, we take the zero frequency limit of the magnetic part of the DMFT self-energy and add it to the spin-averaged QSGW Hamiltonian [20]. As it is clearly shown in Table II and Fig. 4, this static Hamiltonian reproduces very accurately magnetic moment and details of the band structure. This is a strong indication that for Ni the dynamics of local spin fluctuations is not crucial. This will be the case if the quasiparticle picture is a reasonable description of Ni, even if QSGW alone does not contain enough physics to yield an optimum quasiparticle approximation.

To verify this further, we model spin fluctuations by carrying out the QSGW self-consistent cycle in the presence of a magnetic field B^{eff}, and tuning B^{eff} to reduce M (see inset, Fig. 4) Our key finding is that when B^{eff} is tuned to make M agree with experiment, ΔE_x does also, reproducing ARPES spectra to high precision in the FL regime, as clearly reported in Fig. 4 and Table II. Both the QSGW and LSDA overestimate M for itinerant systems, but the latter also *underestimates* it in local-moment systems [Fig. 3(b)]. In the LSDA treatment of Ni, these effects cancel and render the moment fortuitously good. When spin fluctuations are folded in through B^{eff}, the LSDA moment becomes too small. This finding must be interpreted as a sign of the superior level of internal consistency in the QSGW theory with respect to LSDA. Without such a degree of consistency spin fluctuations could not be approximated by a static field.

III. CONCLUSIONS

We have performed detailed QSGW calculations of the electronic band structure of several 3d metallic compounds to assess the reliability of this theory in the Fermi liquid regime and the importance of the nonlocal terms in the self-energy.

—***Fe*:** Through de Haas-van Alphen and cyclotron measurements we established that QSGW QP levels at E_F have an error of $\sim$0.05 eV, and effective masses are well described. Comparable precision is found below E_F by comparing to ARPES data, provided final state scattering is taken into account. The QSGW d bandwidth falls in close agreement with ARPES and is approximately 0.75 times that of the LDA (Fig. 1).

If Σ is k-averaged to simulate a local self-energy, the QSGW band structure changes significantly and resembles the LDA. Thus nonlocality in the self-energy is important in transition metals, and its absence explains why LDA+DMFT does not yield good agreement with ARPES [3].

—***Ni*:** QSGW d bandwidths, the t_{2g}-e_g splitting, the s-d alignment, are all in excellent agreement with experiment, while $\langle M \rangle$ and ΔE_x are too large. However through the addition of a uniform static external field QSGW can give both in good agreement, indicating a high level of consistency in the theory, contrary to LSDA in which it is not possible to have both quantities correct at the same time.

To account for spin fluctuations in an *ab initio* framework, we constructed a QSGW+DMFT implementation and we utilized it at different degrees of approximations demonstrating that in itinerant magnets as Ni (i) the dynamics of fluctuations is irrelevant and (ii) their effect can be very well approximated by a static field as long as the nonlocal correlation part is treated accurately.

ACKNOWLEDGMENTS

This work was supported by the Simons Many-Electron Collaboration and EPSRC Grant No. EP/M011631/1. The authors gratefully acknowledge computer resources from the Gauss Centre for Supercomputing e.V. (www.gauss-centre.eu). We also acknowledge the Partnership for Advanced Computing in Europe (PRACE Project No. 2010PA2762)

for awarding us access to the following resources: Curie FN and TN based in France at the Très Grand Centre de Calcul (TGCC), and SuperMUC, based in Germany at Leibniz Supercomputing Centre.

[1] J. Schäfer, M. Hoinkis, E. Rotenberg, P. Blaha, and R. Claessen, Phys. Rev. B **72**, 155115 (2005).
[2] J. Callaway and C. S. Wang, Phys. Rev. B **16**, 2095 (1977).
[3] J. Sánchez-Barriga, J. Fink, V. Boni, I. Di Marco, J. Braun, J. Minár, A. Varykhalov, O. Rader, V. Bellini, F. Manghi, H. Ebert, M. I. Katsnelson, A. I. Lichtenstein, O. Eriksson, W. Eberhardt, and H. A. Dürr, Phys. Rev. Lett. **103**, 267203 (2009).
[4] A. L. Walter, J. D. Riley, and O. Rader, New J. Phys. **12**, 013007 (2010).
[5] L. Hedin, J. Phys.: Condens. Matter **11**, R489 (1999).
[6] T. Kotani, M. van Schilfgaarde, and S. V. Faleev, Phys. Rev. B **76**, 165106 (2007); our code was adapted from the original ecalj code (github.com/tkotani/ecalj).
[7] S. Ismail-Beigi, arXiv:1406.0772.
[8] M. Methfessel, M. van Schilfgaarde, and R. A. Casali, *Electronic Structure and Physical Properties of Solids: The Uses of the LMTO Method*, Lecture Notes in Physics Vol. 535 (Springer-Verlag, Berlin, 2000).
[9] D. R. Baraff, Phys. Rev. B **8**, 3439 (1973).
[10] A. Gold, J. Low Temp. Phys. **16**, 3 (1974).
[11] A. Santoni and F. J. Himpsel, Phys. Rev. B **43**, 1305 (1991).
[12] J. Pendry, Surface Science **57**, 679 (1976).
[13] R. Matzdorf, Surf. Sci. Rep. **30**, 153 (1998).
[14] V. N. Strocov, J. Elec. Spect. Rel. Phenomena **130**, 65 (2003).
[15] V. N. Strocov, R. Claessen, G. Nicolay, S. Hüfner, A. Kimura, A. Harasawa, S. Shin, A. Kakizaki, P. Nilsson, H. Starnberg *et al.*, Phys. Rev. Lett. **81**, 4943 (1998).
[16] P. J. Feibelman and D. Eastman, Phys. Rev. B **10**, 4932 (1974).
[17] S. Tanuma, C. J. Powell, and D. R. Penn, Surf. Interface Anal. **21**, 165 (1994).
[18] A. V. Gold, L. Hodges, P. T. Panousis, and D. R. Stone, Intern. J. Magn. **2**, 357 (1971).
[19] G. G. Lonzarich, in *Electrons at the Fermi Surface*, edited by M. Springford (Cambridge University Press, Cambridge, UK, 1980).
[20] See Supplemental Material at http://link.aps.org/supplemental/10.1103/PhysRevB.95.041112 for further details on the electron-phonon coupling model and on the QS*GW*+DMFT implementation and application to Fe and Ni.
[21] N. W. Ashcroft and D. Mermin, *Solid State Physics* (Saunders College Publishing, Philadelphia, USA, 1976).
[22] K. D. Belashchenko, V. P. Antropov, and N. E. Zein, Phys. Rev. B **73**, 073105 (2006).
[23] F. J. Himpsel, J. A. Knapp, and D. E. Eastman, Phys. Rev. B **19**, 2919 (1979).
[24] K. Karlsson and F. Aryasetiawan, Phys. Rev. B **62**, 3006 (2000).
[25] I. I. Mazin, D. J. Singh, and A. Aguayo, in *Physics of Spin in Solids: Materials, Methods and Applications*, edited by Samed Halilov (Kluwer Academic Publishers, Dordrecht, Netherlands, 2004).
[26] M. Shimizu, Rep. Prog. Phys. **44**, 329 (1981).
[27] W. Eberhardt and E. W. Plummer, Phys. Rev. B **21**, 3245 (1980).
[28] S. Biermann, F. Aryasetiawan, and A. Georges, Phys. Rev. Lett. **90**, 086402 (2003). The main accomplishment of this work was to reproduce within GW+DMFT the satellite at ~ -6 eV. This is also captured by LDA+DMFT [3].
[29] K. Haule, C. H. Yee, and K. Kim, Phys. Rev. B **81**, 195107 (2010).
[30] P. Werner, A. Comanac, L. de Medici, M. Troyer, and A. J. Millis, Phys. Rev. Lett. **97**, 076405 (2006).
[31] K. Haule, Phys. Rev. B **75**, 155113 (2007).
[32] S. Choi, A. Kutepov, K. Haule, M. van Schilfgaarde, and G. Kotliar, npj Quantum Mater. **1**, 16001 (2016).